



Assessment of PMMA and polystyrene based microfluidic chips fabricated using CO₂ laser machining

Ismail Bilican^{a,b}, Mustafa Tahsin Guler^{b,c,*}

^a Science and Technology Application and Research Center, Aksaray University, 68100 Aksaray, Turkey

^b UNAM—National Nanotechnology Research Center, Institute of Materials Science and Nanotechnology, Bilkent University, 06800 Ankara, Turkey

^c Department of Physics, Kirikkale University, 71450 Kirikkale, Turkey

ARTICLE INFO

Keywords:

Microchannels
PMMA
Polystyrene
CO₂ laser

ABSTRACT

Laser machining could be an alternative way for the fabrication of microchannels. In this study, laser machining of polymethylmethacrylate (PMMA) and polystyrene (PS) substrates were characterized in detail. A fabrication method preventing leakage at PS microchannel inlets was developed. The effect of laser parameters (power, speed and frequency) on engraving was analyzed by scanning electron microscopy. Laser ablation mechanism of both materials was explained through thermal analysis and material properties. Defocusing the laser beam was also analyzed as an additional parameter affecting the channel profile. Two parameters affecting the resolution were analyzed which are the minimum channel size that can be achieved by the laser beam and x-y stage of the laser engraver for straight and complex microchannel geometries. The hydrophilicity of the surface before and after laser machining was tested with contact angle measurements. The capabilities/limitations of machining were revealed through some complex channel structures. Finally, a passive micromixer and a droplet generator microfluidic devices were manufactured and tested, and promising results were obtained.

1. Introduction

After the invention of soft lithography in 1998 [1], microfluidics research has increased dramatically. Yet, it still requires cleanroom facilities for device fabrication, making it less accessible for a wider population. Following numerous promising outputs of microfluidics technology, new fabrication methods were developed to reduce the complexity of microchannel fabrication. Xurography [2] proposed a method that cuts a double-sided tape with razor blades by a cutter plotter machine. In microwire molding, a wire with a diameter on the order of a few microns is put on a substrate to form a mold, which is followed by the casting process [3]. Micro milling is done on aluminum or plastic slabs in micron-scale [4]. In pen microfluidics, the ink of a pen is used as a mask layer, and the rest of the plastic sheet is exposed to solvent vapor. The vaporized area swells out while the inked area stays the same forming hollows on the surface, which are the microchannels [5].

Laser machining came up as an alternative method to provide simplicity. The first laser machined microchannel was fabricated using a UV excimer laser in 1997 [6]. Following it, a CO₂ laser source was first employed in 2002 to machine microchannels [7]. Other laser sources used to fabricate microchannels include femtosecond laser [8]

and Nd-yag laser [9]. Comparing all, CO₂ laser machining is advantageous in terms of simplicity; the reason for searching an alternative method to soft lithography. CO₂ laser ablation occurs through thermal energy due to the wavelength of laser beam, being nearly 10 μm. Thus, it is more suitable to process low heat conductive materials (nonmetals) like polymers. Three different ablation mechanisms have been defined for polymers: melt shearing, vaporization and chemical degradation [10]. Of our interest, PMMA and PS ablation are performed by vaporization and chemical degradation, respectively [11].

Studies, focusing on machining and processing of polymeric materials by CO₂ laser, are listed here. Theoretical and experimental comparisons were done for PMMA [12]. Paper machining for microfluidics applications was shown in [13]. The effect of power and velocity of the laser beam is among the most studied subjects [14–16], polycarbonate [17,18] and polystyrene [19] microchannel machining were also shown.

Here, the fabrication of microfluidics device is discussed in numerous aspects. First, the microfluidic chip-to-world connection was explained. A new method is developed for the PS inlet, which normally has a leakage issue when directly connected to a tubing. The effect of defocusing the laser beam is investigated and compared for both materials. Laser speed, power and frequency parameters are also

* Corresponding author at: Department of Physics, Kirikkale University, 71450 Kirikkale, Turkey.

E-mail address: gulermt@gmail.com (M. Tahsin Guler).

<https://doi.org/10.1016/j.apsusc.2020.147642>

Received 13 January 2020; Received in revised form 12 July 2020; Accepted 19 August 2020

Available online 25 August 2020

0169-4332/ © 2020 Elsevier B.V. All rights reserved.

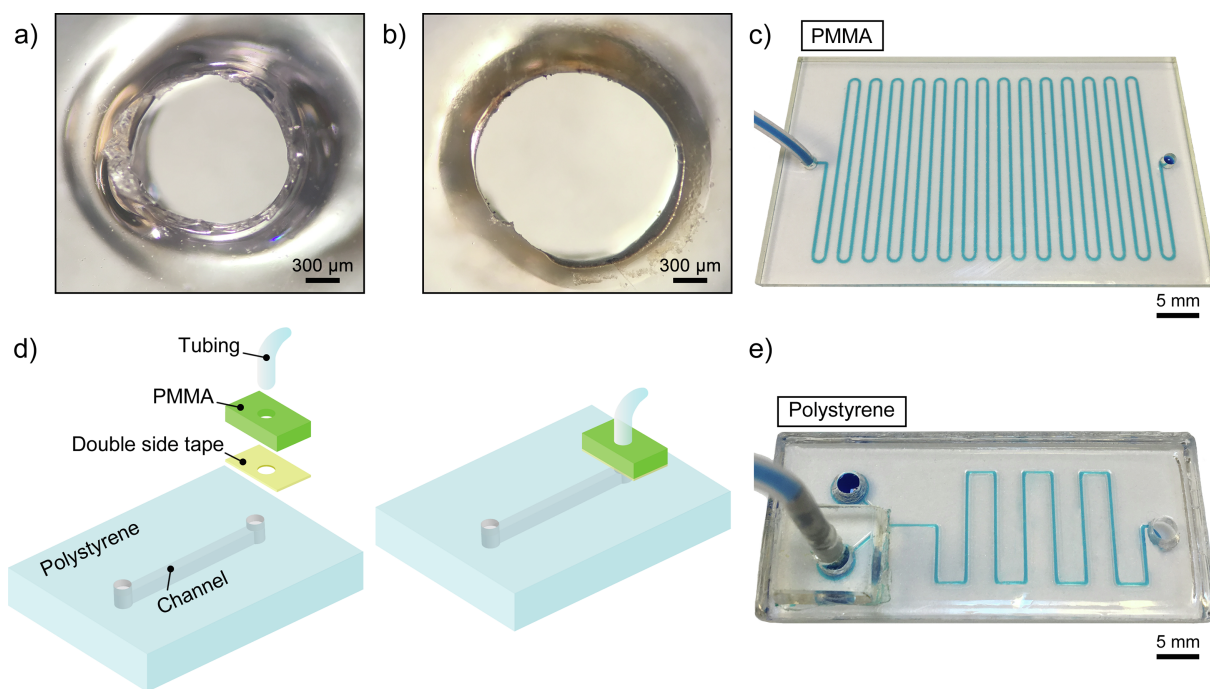


Fig. 1. (a) Laser cut PS inlet, (b) PMMA inlet, (c) PMMA microfluidic chip, (d) a representative drawing that shows the integration of PMMA adaptor to the PS inlet (e) PS microfluidics chip.

investigated. Surface roughness is investigated with scanning electron microscopy (SEM) for both materials. Thermogravimetric analysis (TGA) is done for both materials to elaborate on different features presented in the laser ablation process. Resolution is handled in two ways. One is the basic resolution that only enables to produce preliminary straight microchannels, and the other is valid for all kinds of designs. For sealing the channel, three different tapes are investigated, and leakage pressures are found for different fluids. Since hydrophobicity of the channels is important for various applications, contact angle measurements are performed before and after laser machining. Finally, micromixer and droplet generator applications are done with the laser machined PMMA and PS microchannels.

2. Experimental setup and method

Standard PMMA and PS sheets are ordered from a local supplier. 30 W CO₂ laser (Epilog Zing) is employed for material processing, which has a 10.6 μm wavelength infrared laser source. Throughout the paper, power and speed parameters are given as percentage units. Speed setting regulates the speed of the laser cutter head which is determined as 25.5 mm/s in vertical and 27.1 mm/s in the horizontal axis after the measurement at 100%. Laser pulse duration was measured with a custom made setup as shown in the [Supporting Information](#). According to our findings, pulse duration of the laser is directly proportional with power and inversely disproportional with frequency, which is formulized as follows:

$$\text{Pulse duration: } P/f \quad (1)$$

Here P denotes power in percentage unit and f denotes frequency in Hz. The machining process in this study is carried out in the vector cutting mode of the laser.

For the observation of the surface, SEM images was taken after the gold coating of the plastic surface. Optical microscopy photos of the devices were taken from the binocular of a stereomicroscope (KRUS) with a cellphone. Thermal material characterization of PMMA and PS was realized using thermo gravimetric analysis (TGA) and differential scanning calorimetry (DSC) at nitrogen environment. TGA-DTG analysis were carried out with EXSTAR S11 7300 thermogravimetry

analyzer by heating up the samples from 30 to 700 °C at 10 °C min⁻¹ rate. DSC analysis were realized in TA instruments Q10 for 10 mg of both samples using an aluminum pana from 30 to 280 °C at 10 °C min⁻¹ heating rate. Besides, simultaneous TGA/DSC measurements were carried out with TA Instruments Q600 STD for investigation of absorbed heat till the evaporation in both nitrogen and dry air environment at 10 °C min⁻¹ heating rate. For calculation of the heat from DSC outputs, numerical integration was done with custom written Python code by using the numpy and pandas libraries. Contact angle measurement of the laser machined surfaces were performed (dataphysics, OCA 30) and compared with pre-machined surfaces. Surface roughness measurements were carried out with an atomic force microscopy (AFM) device (Asylum MFP-3D SPM) at 0.6 Hz scanning rate. The scanning was realized in tapping mode using silicon nitride cantilevers with a tip nominal radius of 8 nm (NCLV-A, Bruker) under ambient conditions. Three different tapes were used to seal the microchannels, which are cellophane, scotch crystal and Kapton.

In micromixer application, to observe the mixing of the fluids, deionized (DI) water is mixed with yellow or blue food dye. When the fluids are mixed, green color appears as an indication of mixing. Fluids are sent through the microchannel with a computer-controlled pressure pump (Elve Flow, OB1). The fluid is transferred to the microchannel from the vials with silicon tubing (Cole-Parmer). A metal flat syringe tip is inserted at the end of the tubing to disable collapsing at the channel inlet.

Channel inlets and outlets are opened after the surface machining that forms the microchannels. Since the connection is done with a soft silicone tubing having cylindrical shape, inlets are cut out in circular shape. One of the biggest issues that we encounter in this study is the fluidic connection of the PS channels. The same issue does not occur for PMMA channels. During the laser cutting of PMMA, the material does not melt but only evaporates. Hence, designed circle is cut on PMMA without any defect. Yet, melting takes place in laser cutting of the PS [20]. The melted PS is frozen at noncircular shapes which results in an inaccurate cylindrical shape that also has defects on the sidewall as shown in [Fig. 1\(a\)](#). Therefore, cylindrical tubing does not fit well to the PS inlet causing leakage. We overcome this issue with a novel method

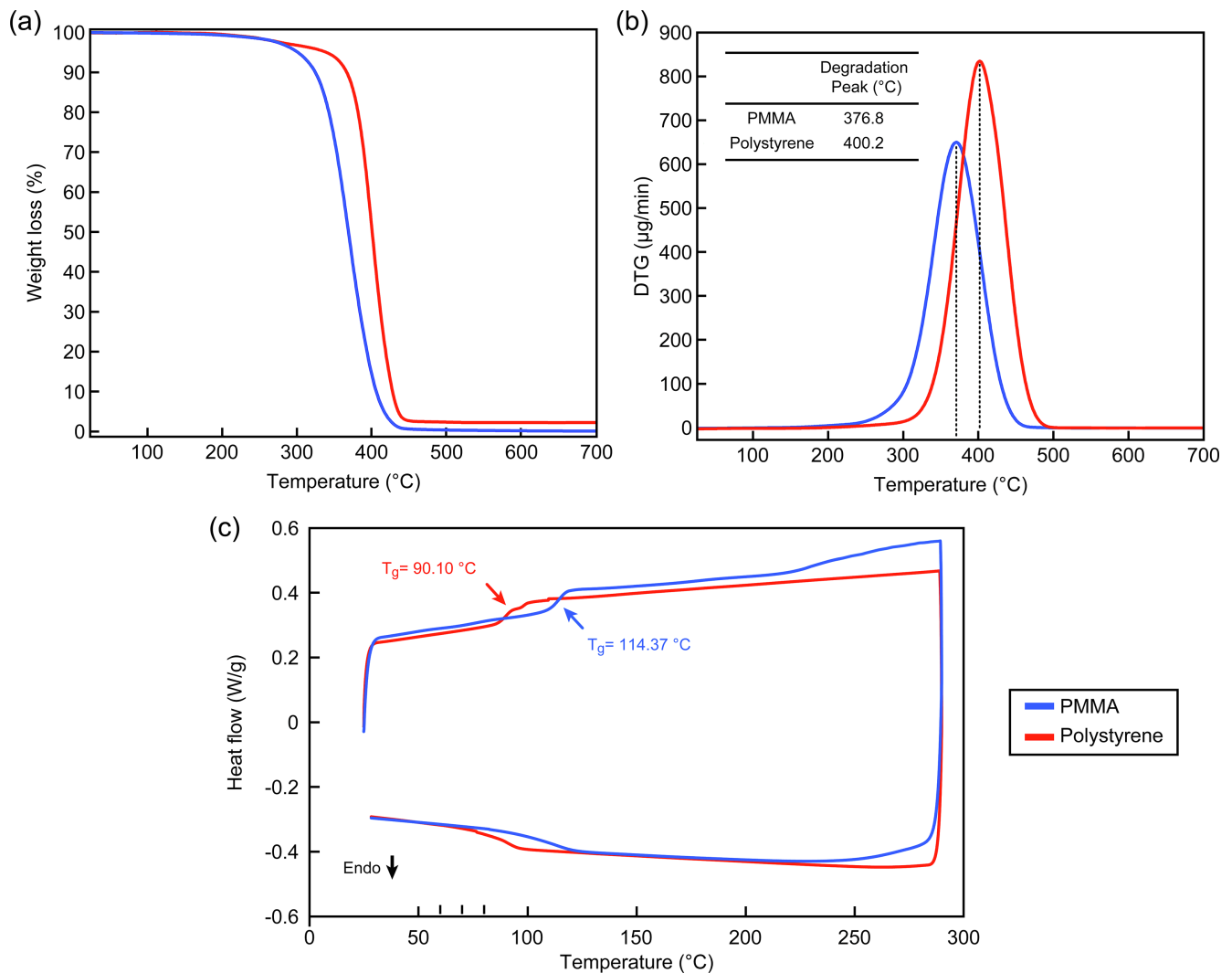


Fig. 2. (a) TGA, (b) DTG and (c) DSC thermograms of PMMA, PS.

by putting a PMMA piece on top of the PS inlet. A small square piece less than 1 cm² is cut from PMMA, following the cutting-out of the cylindrical part from the middle as shown in Fig. 1(b-d). The square PMMA is stuck over the PS inlet with a double-sided tape. Since PMMA enables a perfectly circular cut, the silicon tubing fits very well without any leakage as shown in Fig. 1(e).

3. Results and discussions

3.1. Thermal characterization of the materials

TGA, DTG and DSC thermograms are shown in Fig. 2. As shown in the literature previously, a single degradation step was observed for PMMA and PS [21,22]. Ash contents of PMMA and PS were recorded as 0% and 2.8% respectively at 700 °C. As shown in Fig. 2(b), degradation peaks are observed at 376.8 °C, 400.2 °C for PMMA and PS respectively. With regards to DTGmax values, PS is more thermally durable than the PMMA. As shown in Fig. 2(c), glass transition temperature (T_g) of PMMA and PS are 114.4 and 90.1 respectively that are consistent with the previous literature [23,24].

3.2. Investigation of laser ablation

The laser ablation is a thermal diffusion and evaporation process with a special heat source, which is the laser beam focused on the

material [12]. Hence, the heat conduction of the laser ablation process in a material can be given as follows:

$$\frac{\partial^2 T}{\partial x^2} + \frac{\partial^2 T}{\partial y^2} + \frac{\partial^2 T}{\partial z^2} - \frac{\rho c_p}{k} \frac{\partial T}{\partial t} = -\frac{I}{k} \quad (2)$$

Here T denotes the temperature at a point (x,y,z), I is the laser power, k is thermal conductivity, ρ is density, and c_p is specific heat. Once the material reaches the evaporation temperature according to Eq. (2), it leaves the surface taking all the absorbed energy. The amount of energy to be absorbed for evaporation depends on the material properties. DSC analysis of the both materials reveals the heat energy requirement for evaporation. For detecting the thermal degradation while measuring the absorbed heat simultaneously, TGA/DSC analysis is carried out together. Therefore, simultaneous TGA/DSC measurement provides a good platform in analysis of the ablation process with a drawback that is time scale. In pulsed laser ablation, heating and evaporation occurs in the interval between the beginning and ending of the laser pulse, which is on the order of milisecond for our case while it is around 60 min in the DSC. The results of TGA/DSC analysis of both materials indicate that the degradation process differs depending on to dry air and nitrogen environment as shown in Fig. 3. Since the laser ablation takes place in air environment, TGA/DSC output in dry air environment represent laser machining process better. Integration of heatflow curve over time axis from the room temperature to the point where the materials evaporations are complete, which are 403 and 522 °C for PMMA

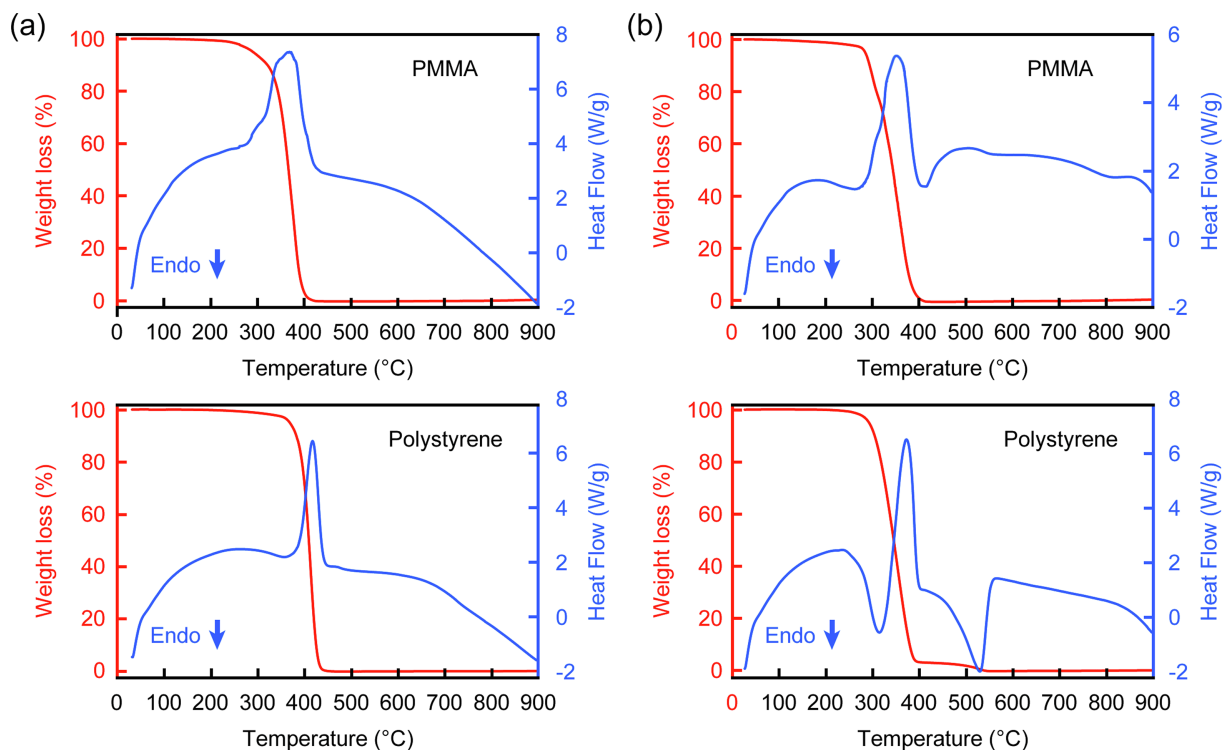


Fig. 3. Simultaneous TGA/DSC analysis of PMMA and PS (a) nitrogen environment (b) dry air environment.

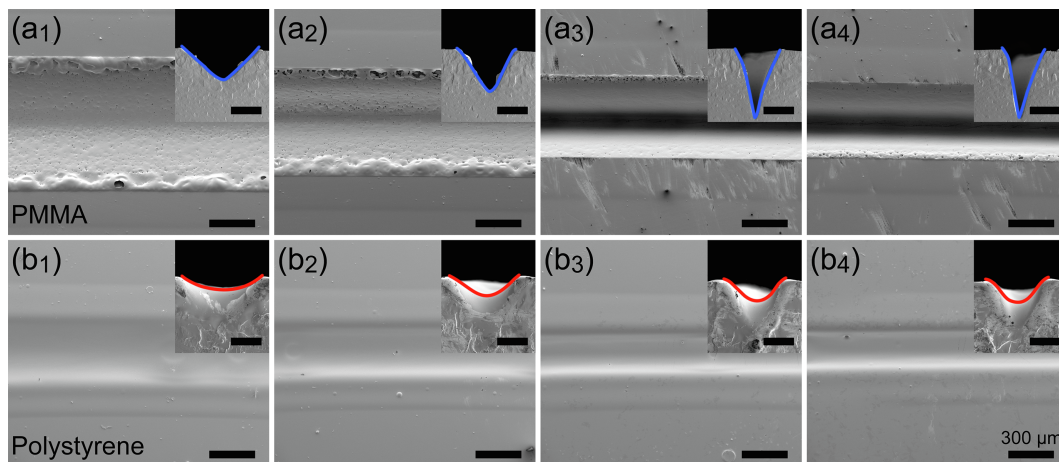


Fig. 4. Effect of defocusing on microchannel profile. (a1) 9 mm, (a2) 6 mm, (a3) 3 mm, (a4) 0 mm defocused engraving of the channels for PMMA; (b1) 9 mm, (b2) 6 mm, (b3) 3 mm, (b4) 0 mm defocused engraving of the channels for PS.

and PS respectively, produces the total heat energy to be absorbed. Numerical integration gives 4263.1 and 4311.8 j/g for PMMA and PS respectively. Although there is a significant difference in ablation amount between the two materials, DSC measurement shows that the heat requirement to be absorbed for evaporation is slightly different for both materials. According to our experimental results, there is 20% weight difference in ablation of PMMA and PS at 30% speed and power and 1 kHz. The reason of the gap between the ablation ratios is due to the quite different thermal conductivities of the both materials, which are $0.21 \text{ Wm}^{-1}\text{K}^{-1}$, $0.33 \text{ Wm}^{-1}\text{K}^{-1}$ for PMMA and PS respectively [25,26]. Higher thermal conductivity leads to faster diffusion of the absorbed laser energy inside the material. Therefore, the diffuse energy waste inside the material instead of condensation to a point and inducing ablation.

The thermal conductivity also defines the channel shape which is wider in PS and deeper in PMMA. Higher thermal conductivity of PS

lead to more diffusion of heat and homogenous ablation in all direction. On the other hand, lower thermal conductivity of PMMA reduces the heat diffusion yielding ablation in the shape of laser beam. Fig. 3 clearly illustrate the disparity of ablation in shapes for PMMA and PS. Our laser has pulse duration is around 10^{-4} s; for laser material processing independent from heat diffusion, ultra short pulse lasers are ideal that are capable of even metal processing [27].

3.3. Effect of defocusing

The laser beam is normally focused on the workpiece to achieve highly concentrated energy on a narrower area for better ablation. Instead of cutting, our purpose is machining the surface, which removes the need for a focused laser beam. The effect of defocusing was previously shown for PMMA [28]. Raising the workpiece from the focal point towards the moving head by putting 3 mm thick plates to the

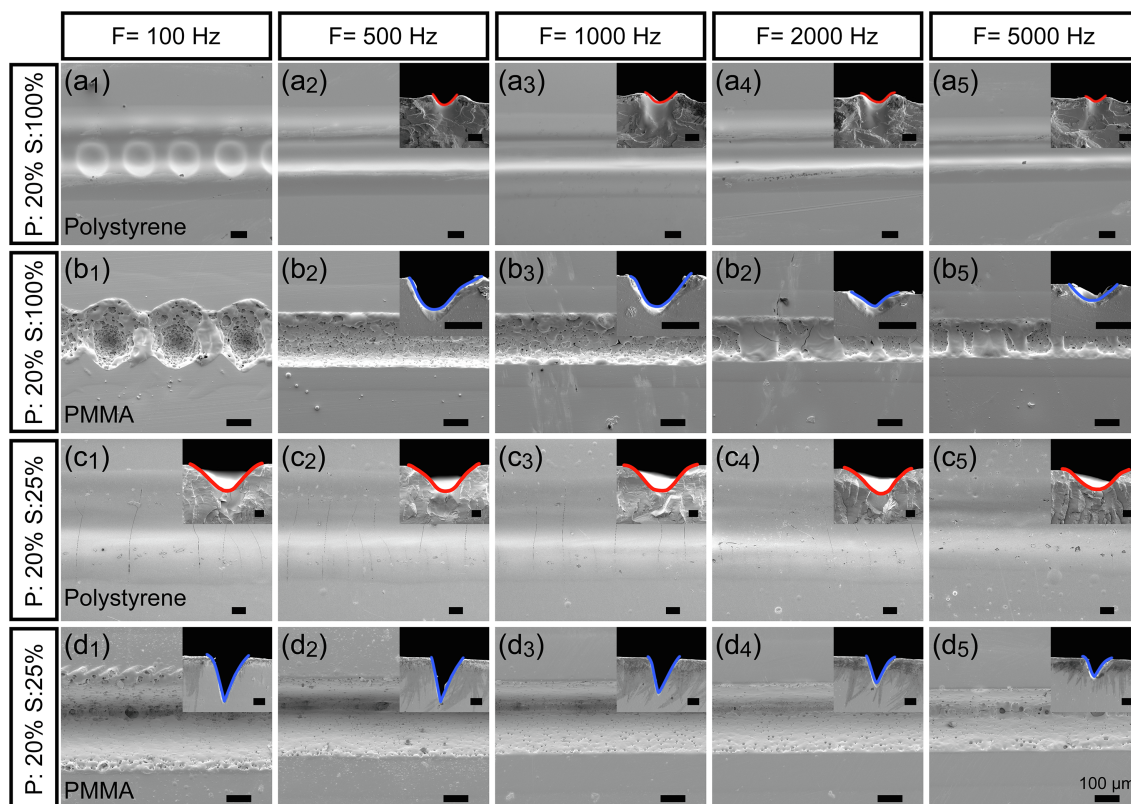


Fig. 5. Profile and top view SEM images of PMMA and PS for various power (P), speed (S) and frequency (F) settings. All the scale bars are 100 μm.

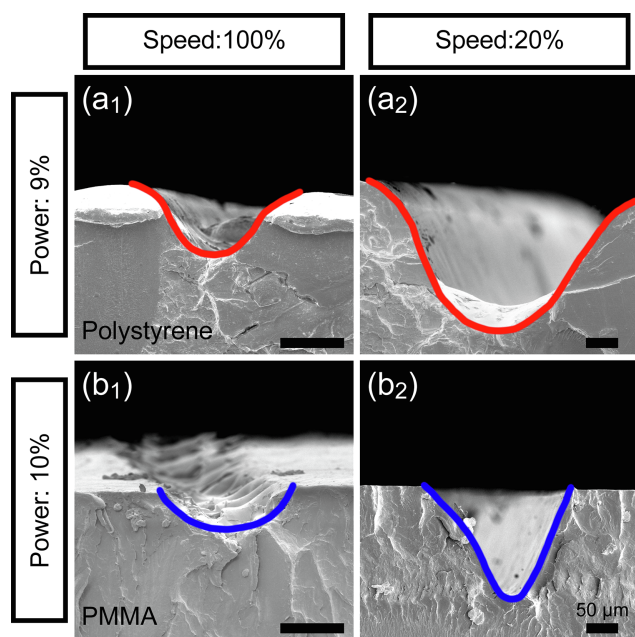


Fig. 6. Minimum channel sizes of PMMA and PS for preliminary and complex designs. (a1), (b1) are the minimum size that is valid for engraving simple straight channels. (a2), (b2) are the minimum channel size that is valid for all kind of complex designs.

under brings it to a defocused regime of the laser beam with a precise millimetric control. The channel engraving is done at three different heights from the focal point that are 3, 6 and 9 mm. Power, speed and frequency rates are set to 3 W, 5 mm/s and 5 kHz, respectively. It can be seen from Fig. 4 that the channel depth decreases, and the channel width increases due to defocusing for both materials. Defocusing can be

used as an additional parameter to regulate the width/depth ratio of the channels. Due to the Gaussian shape of the laser beam, the channel profile is achieved in Gaussian shape as well. On the other hand, a rectangular channel profile is possible with a previously fabricated metal mask [29] on bulk material. It is also possible via the machining of the spin-coated polydimethylsiloxane (PDMS) layer [30,31].

Since the channel profile geometry is important in some branches of microfluidics like inertial microfluidics in trapezoidal [32], triangular [33] shapes or biomimetic applications in semicircular [34] shapes, defocusing might be a significant additional parameter of laser machining. Channel profile is also important for the switching of microvalves in microchannels. Some microvalves require smooth hemispherical channel profile geometries rather than cornered to work efficiently. Membrane valve [35] is a good example that cannot work on the channels as shown in Fig. 4(a3, a4) that can only work on smoother shapes. Yet, some microvalves do not have any specific shape requirement and can work in all kinds of channel geometries [36] with different advantages and disadvantages.

According to the SEM results, PS engraving ends up with very smooth surfaces, unlike PMMA. PS ablation mechanism consists of two steps as shown in Fig. 3 TGA/DSC. The ablation is via sublimation in PMMA; hence, the material is directly evaporated from the solid phase, skipping the intermediate liquid phase. Due to sublimation, the PMMA surface is rougher after the ablation in comparison to PS, where 2.8% of material remains after first melting and evaporation step. Since the evaporation of the remaining material takes place in 395–522 °C range, which is relatively high, it resolidifies after laser pulse passes forming a smooth surface. The molecular weight of the polymer has also an effect on surface roughness [37]. It is shown that the surface roughness can be improved by initial heating of PMMA [38].

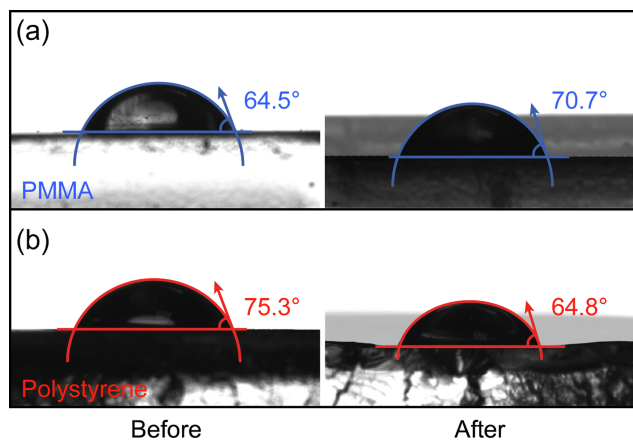
3.4. Effect of power, speed and frequency on engraving

PS and PMMA are engraved at different settings of power, speed and

Table 1

Leakage pressure (mbar) of cellophane, Scotch Crystal and Kapton tapes in PMMA and PS microchannels for DI water, IPA and Silicon oil.

	Cellophane Tape		Scotch Crystal		Kapton Tape	
	PMMA	PS	PMMA	PS	PMMA	PS
DI water	900	500	1500	900	>2000	1800
IPA	70	30	180	95	400	205
Silicon oil	850	480	1500	890	>2000	1700

**Fig. 7.** Contact angle measurement of (a) PMMA and (b) PS before and after laser machining.**Table 2**

Surface roughness of PMMA and PS before and after laser machining.

Samples	Surface roughness (nm)	
	Before	After
Polystyrene	3.319 ± 0.992	1.327 ± 0.658
PMMA	1.205 ± 0.243	8.816 ± 2.653

frequency. At low frequency and high speed, the pulsed character of the laser beam is seen on the surface. Fig. 5(a₁, b₁) show circular cavities that are engraved by the laser where the speed is too high for pulse fired to the surface with 10 ms periods which reveals the pulsed character of the laser beam. When the speed is reduced to one-fourth of the previous value as shown in Fig. 5(c₁, d₁), the periodic character of the laser disappears at the same frequency.

The frequency of the laser affects the channel size. This observation is clear in Fig. 5 when inspected from left to right in each line of sub-figures. At the same speed and power settings, any rise in the frequency ends up with a reduction in the channel size. Both materials present the same feature with regard to frequency. Some groups investigated the frequency in a different unit which is pulse per inch (PPI). Those groups mainly focused on the surface properties related to PPI [30], but only Prakash et al. [39] investigated the effect on channel size, which asserts PPI as a non-effective parameter. However, our findings are different as shown in Fig. 5.

The additional experiment is carried out to better demonstrate the effect of the frequency. Fig. S3 shows the ablation of PMMA at a wide range of frequencies. As the frequency increases from 10 Hz onwards, the hole size decreases due to the reduction of the pulse period of the laser. Above 100 Hz, the heat-affected zone of each pulse starts to merge. As the frequency increases, pulse duration decreases, reducing the heating effect. This is apparent from the hole size in Fig. S3. With increasing frequency, energy and period of the laser pulses decrease.

The laser pulses also do not completely overlap each other. Since the energy is low, it cannot be so effective. In addition, the following pulse does not hit the same point. It hits slightly next spot after a short period. Therefore, at high frequency, the laser beam starts ablation which ends rapidly and left that spot of the material hot. Hence, some of the energy is consumed in heating since the energy is interrupted just after starting the ablation. Then the surface is left to cool down convectively because the laser head has already moved to the next position. Therefore, more energy is wasted for heating instead of ablation at higher frequencies. This fact causes shrinkage in the channel size as shown in Fig. 4 and Fig. S3.

As another parameter, speed has two different effects on the ablation process. One is the total amount of the energy transferred to the surface, which changes with the speed as the energy parameter is set in the power unit. When the same process is done at the same power but different speed settings, the total energy transfer would be lower at a higher speed setting which changes the ablation rate. The other effect is about the overlapping of the laser pulses which is discussed above.

3.5. Resolution of machining

Minimum channel size is another important parameter in microfluidic applications. For example, it defines the limitations of a microchip in terms of sensitivity if it is to be used in a sensing application. A channel used in a bacteria sensing application [40,41] should be nearly three times smaller than a channel used in blood cell sensing applications [42,43]. Besides, channel size is critical for particle manipulation [44] with inertial microfluidics or viscoelastic fluids [45]. Here are shown two resolution values that are valid for different purposes. One is true for only a simple linear channel, which is done by a single pass of the laser. The other resolution value is true for all kinds of designs including both simple and complex geometries. As shown in Fig. S4, complex designs cannot be done properly above 20% speed settings. When speed is too high, engraving does not match with the drawing due to delays coming from the switching time of the laser beam. Thus, 100 μm height and 30 μm width can be achieved for PMMA, and 50 μm height and 100 μm width can be achieved for PS for single straight channels; 200 μm height and 250 μm width can be achieved for PMMA and 250 μm height and 300 μm width can be achieved for PS. Fig. 6 shows the results for PMMA and PS at 5 KHz.

3.6. Microchannel sealing

The sealing of the microchannel is a big issue and still open to discussion. There are numerous ways in the sealing of hard plastic channels for PS and PMMA [46]. It is generally the thermal bonding of the same material over the machined piece. Sealing the microchannels with tape is a new trend in the microfluidics community [47]. We have adopted the tape sealing for the sake of simplicity, which deserves more investigation. Three different types of transparent tapes are used and tested at several conditions. Sealing performance, referring to pressure resistivity, is investigated for different liquids for PMMA and PS. According to the results in Table 1, the best sealing is performed by Kapton tape. Leakage pressure is nearly the same for silicon oil and DI

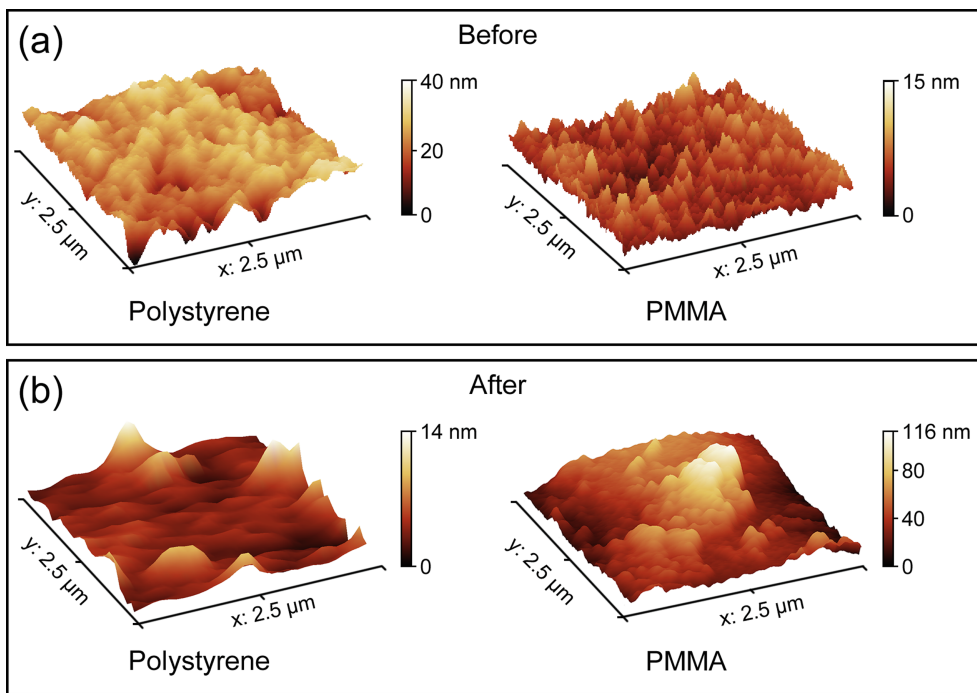


Fig. 8. AFM images of PS and PMMA (a) before laser machining (b) after laser machining.

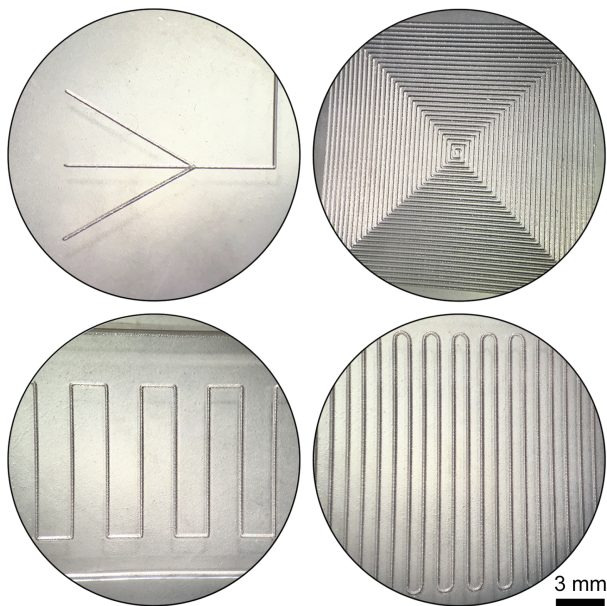


Fig. 9. Top views of different designs machined by the laser on PMMA surface.

water. Isopropyl alcohol (IPA) leaks at relatively lower pressure values than the others. In addition, PMMA stands at higher pressure values than PS. The pressure test is done using the chips shown in Table 1 that are engraved at 10% power, 20% speed and 5 kHz frequency for PMMA and PS.

3.7. Surface wettability

Hydrophobicity is also very important like surface roughness. A contact angle measurement test is carried out for inspection before and after laser treatment of the surface. The critical value for the contact angle is 90°. A higher value indicates a hydrophobic surface characteristic whereas a lower value implies a hydrophilic surface [48]. According to the results shown in Fig. 7, PMMA and PS surfaces are

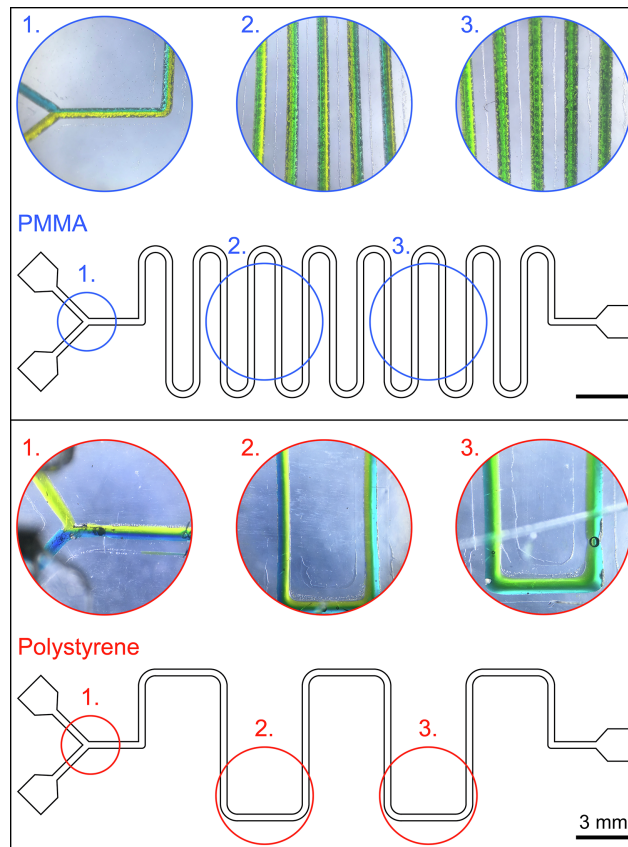


Fig. 10. Passive mixer made of PMMA and PS where blue and yellow dye fluids are mixed, giving green color.

hydrophilic before the laser treatment. The whole surface of 1 cm² plastic pieces is processed at 10% power, 30% speed and 5 kHz frequency settings. After laser processing, PMMA loses hydrophilicity while PS gains hydrophilicity. Both materials are hydrophilic before

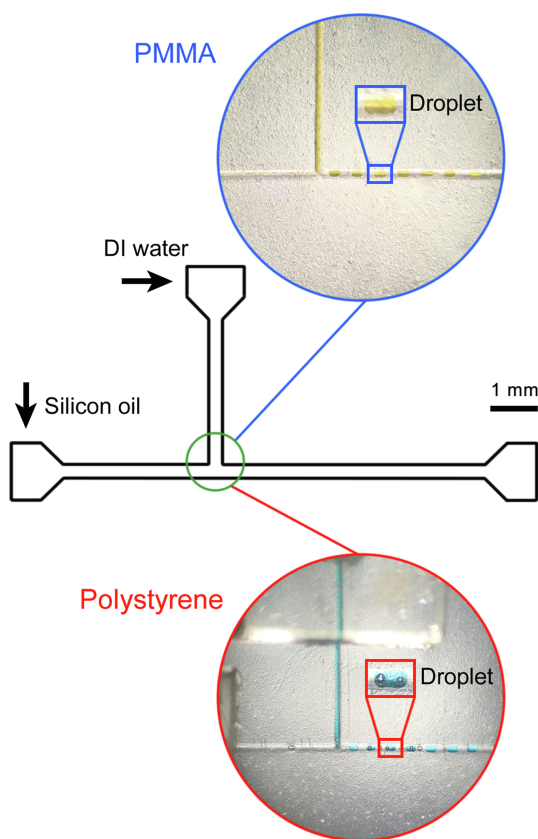


Fig. 11. Droplet generation experiment in a T-junction geometry for PMMA and PS microchannels.

and after laser processing, which means microchannels engraved in to PMMA and PS will be hydrophilic. We think that PMMA loses hydrophilicity after machining due to direct sublimation during the ablation, which increases surface roughness. Since surface roughness decreases in PS following the laser machining due to resolidifying materials, it gain hydroflicity.

3.8. Surface roughness

Surface roughness measurements were done with AFM whose results are given at Table 2 and Fig. 8. PMMA and PS substrates were analyzed before and after the laser machining. According to the results, surface roughness increases after the laser machining at PMMA which is due to the fact that the PMMA directly sublimate during the ablation. As the heat diffusion process is random in nanoscale like all the other diffusion processes, the PMMA surface is etched randomly on the atomic scale as well leading to higher surface roughness. In contrary to PMMA, PS ablation consists of two steps of which the second one occurs at higher temperature. Since the laser beam can not ablate the whole material at the mentioned speed and power settings, there leave some material at liquid state after laser passes which resolidify later. Hence the remaining surface becomes planer then before ablation.

3.9. Applications

It is possible to fabricate all kinds of geometries with laser machining as long as we stay in the limits of the resolution. There are two kinds of resolution: the resolution of the x-y stage and the minimum size of the laser ablation of the channels. The precision of the laser ablation is a few hundred μm . Yet, the maximum resolution of the x-y stage is 1000 dpi which is equal to 24 μm . These limits enable the edges of the two ablation areas to be as close as 24 μm with the line width no lesser

than 100 μm . Several designs including intersections, curved and flat turnings and intensive channels are machined as shown in Fig. 9.

Mixing of the fluids in a low Reynolds number is one of the biggest issues of microfluidics. There are some active mixing methods [49–51] that require additional components to the chip increasing complexity and cost. On the other hand, passive mixing does not require any additional components that work based on diffusion. Since diffusion needs time in proportional to distance, a long channel is designed to provide enough time for two fluids to mix. Here, two passive mixers are made of PMMA and PS by laser machining as shown in Fig. 10. In the intersection, blue and yellow dyed fluids do not mix in the laminar flow regime. While the fluids progress inside the channels, both start to mix, forming green dye because of diffusion. At the region close to the outlet, two fluids are totally mixed, which is evident from the green color covering the whole channel. It can be seen PS is a good candidate for applications requiring optical transparency.

Droplet formation is one of the most promising applications of microfluidics. Droplets can be set to nano to picoliters in volume [52], which enables highly sensitive detection. From blood typing [53] to PCR [54], several sensing applications can be added to the list [55]. In addition to sensing applications, chemical synthesis is another area of application that lowers the consumption of expensive reagents [56]. Therefore, a fabrication method should be able to make a microchannel that is capable of producing droplets. In Fig. 11, the production of microdroplets are shown for PMMA and PS microchannels. There is one additional point. According to our previous experience of droplet formation in PDMS microchannels, droplet generation is harder in PMMA and PS microchannel. It is harder to find the right pressure values, and it takes more time for steady-state. This is true at least for T-junction. Y-junction might be better for droplet generation in laser cut plastic channels as shown in [19].

4. Conclusion

We have shown that CO_2 laser machining of PMMA and PS might be a good alternative of the clean room based fabrication methods overcoming complexity and cost issues. The advantages and disadvantages of the machining of both materials were revealed as follows: Due to the melting step during the ablation of PS, a good sealing in the inlets of the microfluidics chips cannot be achieved unlike PMMA. Therefore, a method was developed to achieve a good sealing between tubings and the inlet hole by attaching a PMMA piece via double-sided tape. Down to 30/100 μm width/height and 50/100 μm width/height can be achieved for PMMA, PS with this laser machining method. We found out that when the laser frequency increases, ablation efficiency decreases. In other words, lower frequencies ablate more material at the same power setting. Sealing of the microchannel was made through the tape as a low-cost alternative to other methods. Leakage tests were performed for all tapes using different liquids. As a result, Kapton tape gave the best sealing performance. IPA was the liquid hardest to work with in terms of lower leakage pressure threshold. As SEM and stereo microscopy photos revealed, PS was clear nearly as much as glass. The only disadvantage of PS was the bubbles formed inside microchannel during the ablation process. While the PMMA channel was not as optically clear as PS, it had a better sealing performance with tape. In addition, it does not require additional processes for the connection of tubings to the inlet. Both materials showed a hydrophilic character before and after laser machining. A passive micromixer and droplet generator on a T-junction, which are among the most common microfluidic techniques, were shown to test the application performance of the laser machined PS and PMMA microchannels giving promising results.

CRediT authorship contribution statement

Ismail Bilican: Conceptualization, Formal analysis, Methodology,

Investigation, Writing - original draft, Writing - review & editing, Visualization. **Mustafa Tahsin Guler:** Conceptualization, Formal analysis, Methodology, Investigation, Writing - original draft, Writing - review & editing, Supervision.

Declaration of Competing Interest

The authors declare that they have no known competing financial interests or personal relationships that could have appeared to influence the work reported in this paper.

Appendix A. Supplementary data

Supplementary data to this article can be found online at <https://doi.org/10.1016/j.apsusc.2020.147642>.

References

- [1] D.C. Duffy, J.C. McDonald, O.J. Schueller, G.M. Whitesides, Rapid prototyping of microfluidic systems in poly (dimethylsiloxane), *Anal. Chem.* 70 (1998) 4974–4984.
- [2] D.A. Bartholomeusz, R.W. Boutté, J.D. Andrade, Xurography: rapid prototyping of microstructures using a cutting plotter, *J. Microelectromech. Syst.* 14 (2005) 1364–1374.
- [3] Y. Jia, J. Jiang, X. Ma, Y. Li, H. Huang, K. Cai, S. Cai, Y. Wu, PDMS microchannel fabrication technique based on microwire-molding, *Chin. Sci. Bull.* 53 (2008) 3928–3936.
- [4] R. Lopes, R.O. Rodrigues, D. Pinho, V. Garcia, H. Schütte, R. Lima, S. Gassmann, Low cost microfluidic device for partial cell separation: Micromilling approach, in: 2015 IEEE International Conference on Industrial Technology (ICIT), IEEE, 2015, pp. 3347–3350.
- [5] O. Rahmanian, D.L. DeVoe, Pen microfluidics: rapid desktop manufacturing of sealed thermoplastic microchannels, *Lab Chip* 13 (2013) 1102–1108.
- [6] M.A. Roberts, J.S. Rossier, P. Bercier, H. Girault, UV laser machined polymer substrates for the development of microdiagnostic systems, *Anal. Chem.* 69 (1997) 2035–2042.
- [7] H. Klank, J.P. Kutter, O. Geschke, CO₂-laser micromachining and back-end processing for rapid production of PMMA-based microfluidic systems, *Lab Chip* 2 (2002) 242–246.
- [8] R. Suriano, A. Kuznetsov, S.M. Eaton, R. Kiyan, G. Cerullo, R. Osellame, B.N. Chichkov, M. Levi, S. Turri, Femtosecond laser ablation of polymeric substrates for the fabrication of microfluidic channels, *Appl. Surf. Sci.* 257 (2011) 6243–6250.
- [9] S.-J. Qin, W.-J. Li, Micromachining of complex channel systems in 3D quartz substrates using Q-switched Nd: YAG laser, *Appl. Phys. A* 74 (2002) 773–777.
- [10] J. Powell, CO₂ laser cutting, Springer, 1993.
- [11] F. Caiazzo, F. Curcio, G. Daurelio, F.M.C. Minutolo, Laser cutting of different polymeric plastics (PE, PP and PC) by a CO₂ laser beam, *J. Mater. Process. Technol.* 159 (2005) 279–285.
- [12] D. Yuan, S. Das, Experimental and theoretical analysis of direct-write laser micromachining of polymethyl methacrylate by CO₂ laser ablation, *J. Appl. Phys.* 101 (2007) 024901.
- [13] J. Nie, Y. Liang, Y. Zhang, S. Le, D. Li, S. Zhang, One-step patterning of hollow microstructures in paper by laser cutting to create microfluidic analytical devices, *Analyst* 138 (2013) 671–676.
- [14] D. Snakenborg, H. Klank, J.P. Kutter, Microstructure fabrication with a CO₂ laser system, *J. Micromech. Microeng.* 14 (2003) 182.
- [15] J.P. Davim, N. Barricas, M. Conceicao, C. Oliveira, Some experimental studies on CO₂ laser cutting quality of polymeric materials, *J. Mater. Process. Technol.* 198 (2008) 99–104.
- [16] J.P. Davim, C. Oliveira, N. Barricas, M. Conceição, Evaluation of cutting quality of PMMA using CO₂ lasers, *Int. J. Adv. Manufact. Technol.* 35 (2008) 875–879.
- [17] X. Chen, Z. Hu, An effective method for fabricating microchannels on the polycarbonate (PC) substrate with CO₂ laser, *Int. J. Adv. Manufact. Technol.* 92 (2017) 1365–1370.
- [18] H. Qi, T. Chen, L. Yao, T. Zuo, Micromachining of microchannel on the polycarbonate substrate with CO₂ laser direct-writing ablation, *Opt. Lasers Eng.* 47 (2009) 594–598.
- [19] H. Li, Y. Fan, R. Kodzius, I.G. Foulds, Fabrication of polystyrene microfluidic devices using a pulsed CO₂ laser system, *Microsyst. Technol.* 18 (2012) 373–379.
- [20] F. Darain, K.L. Gan, S.C. Tjin, Antibody immobilization on to polystyrene substrate—on-chip immunoassay for horse IgG based on fluorescence, *Biomed. Microdevices* 11 (2009) 653–661.
- [21] C.-F. Kuan, W.-H. Yen, C.-H. Chen, S.-M. Yuen, H.-C. Kuan, C.-L. Chiang, Synthesis, characterization, flame retardance and thermal properties of halogen-free expandable graphite/PMMA composites prepared from sol–gel method, *Polym. Degrad. Stab.* 93 (2008) 1357–1363.
- [22] J.D. Peterson, S. Vyazovkin, C.A. Wight, Kinetics of the thermal and thermo-oxidative degradation of polystyrene, polyethylene and poly (propylene), *Macromol. Chem. Phys.* 202 (2001) 775–784.
- [23] K. Aouachria, N. Belhaneche-Bensemra, Miscibility of PVC/PMMA blends by vicat softening temperature, viscometry, DSC and FTIR analysis, *Polymer testing* 25 (2006) 1101–1108.
- [24] C.d.S. Meireles, G.R. Filho, R.M. de Assunção, M. Zeni, K. Mello, Blend compatibility of waste materials—cellulose acetate (from sugarcane bagasse) with polystyrene (from plastic cups): diffusion of water, FTIR, DSC, TGA, and SEM study, *Journal of Applied Polymer Science*, 104 (2007) 909–914.
- [25] M. Mohammadi, J. Davoodi, Thermal diffusivity of PMMA/Alumina Nano Composites Using Molecular Dynamic Simulation, arXiv preprint arXiv:1710.01540, (2017).
- [26] D.R. Lide, *CRC handbook of chemistry and physics*, CRC Press, 2004.
- [27] B.N. Chichkov, C. Momma, S. Nolte, F. Von Alvensleben, A. Tünnermann, Femtosecond, picosecond and nanosecond laser ablation of solids, *Appl. Phys. A* 63 (1996) 109–115.
- [28] L. Romoli, G. Tantussi, G. Dini, Experimental approach to the laser machining of PMMA substrates for the fabrication of microfluidic devices, *Opt. Lasers Eng.* 49 (2011) 419–427.
- [29] S. Prakash, S. Kumar, Fabrication of rectangular cross-sectional microchannels on PMMA with a CO₂ laser and underwater fabricated copper mask, *Opt. Laser Technol.* 94 (2017) 180–192.
- [30] H.-B. Liu, H.-Q. Gong, Templateless prototyping of polydimethylsiloxane microfluidic structures using a pulsed CO₂ laser, *J. Micromech. Microeng.* 19 (2009) 037002.
- [31] Z. Isiksacan, M.T. Guler, B. Aydogdu, I. Bilican, C. Elbuken, Rapid fabrication of microfluidic PDMS devices from reusable PDMS molds using laser ablation, *J. Micromech. Microeng.* 26 (2016) 035008.
- [32] G. Guan, L. Wu, A.A. Bhagat, Z. Li, P.C. Chen, S. Chao, C.J. Ong, J. Han, Spiral microchannel with rectangular and trapezoidal cross-sections for size based particle separation, *Sci. Rep.* 3 (2013) 1475.
- [33] J.-A. Kim, J. Lee, C. Wu, S. Nam, D. Di Carlo, W. Lee, Inertial focusing in non-rectangular cross-section microchannels and manipulation of accessible focusing positions, *Lab Chip* 16 (2016) 992–1001.
- [34] J.S. Choi, Y. Piao, T.S. Seo, Fabrication of a circular PDMS microchannel for constructing a three-dimensional endothelial cell layer, *Bioprocess Biosyst. Eng.* 36 (2013) 1871–1878.
- [35] T. Thorsen, S.J. Maerkl, S.R. Quake, Microfluidic large-scale integration, *Science* 298 (2002) 580–584.
- [36] M.T. Guler, P. Beyazkılıç, C. Elbuken, A versatile plug microvalve for microfluidic applications, *Sens. Actuators, A* 265 (2017) 224–230.
- [37] N.C. Nayak, Y. Lam, C. Yue, A.T. Sinha, CO₂-laser micromachining of PMMA: the effect of polymer molecular weight, *J. Micromech. Microeng.* 18 (2008) 095020.
- [38] Y. Huang, S. Liu, W. Yang, C. Yu, Surface roughness analysis and improvement of PMMA-based microfluidic chip chambers by CO₂ laser cutting, *Appl. Surf. Sci.* 256 (2010) 1675–1678.
- [39] S. Prakash, S. Kumar, Fabrication of microchannels on transparent PMMA using CO₂ Laser (10.6 μm) for microfluidic applications: An experimental investigation, *Int. J. Precis. Eng. Manuf.* 16 (2015) 361–366.
- [40] M.T. Guler, I. Bilican, Capacitive detection of single bacterium from drinking water with a detailed investigation of electrical flow cytometry, *Sens. Actuators, A* 269 (2018) 454–463.
- [41] I. Bilican, T. Bahadır, K. Bilgin, M.T. Guler, Alternative screening method for analyzing the water samples through an electrical microfluidics chip with classical microbiological assay comparison of *P. aeruginosa*, *Talanta* (2020) 121293.
- [42] M.T. Guler, I. Bilican, S. Agan, C. Elbuken, A simple approach for the fabrication of 3D microelectrodes for impedimetric sensing, *J. Micromech. Microeng.* 25 (2015) 095019.
- [43] I. Bilican, M.T. Guler, M. Serhatlioglu, T. Kirindi, C. Elbuken, Focusing-free impedimetric differentiation of red blood cells and leukemia cells: A system optimization, *Sens. Actuators, B: Chem.* (2020) 127531.
- [44] S. Stavrakis, G. Holzner, J. Choo, A. DeMello, High-throughput microfluidic imaging flow cytometry, *Curr. Opin. Biotechnol.* 55 (2019) 36–43.
- [45] M. Asghari, M. Serhatlioglu, B. Ortaç, M.E. Solmaz, C. Elbuken, Sheathless microfluidic cytometry using viscoelastic fluids, *Sci. Rep.* 7 (2017) 12342.
- [46] X. Chen, T. Li, J. Shen, CO₂ laser ablation of microchannel on PMMA substrate for effective fabrication of microfluidic chips, *Int. Polym. Proc.* 31 (2016) 233–238.
- [47] Y. Ren, S. Ray, Y. Liu, Reconfigurable acrylic-tape hybrid microfluidics, *Sci. Rep.* 9 (2019) 4824.
- [48] Y. Ma, X. Cao, X. Feng, Y. Ma, H. Zou, Fabrication of super-hydrophobic film from PMMA with intrinsic water contact angle below 90, *Polymer* 48 (2007) 7455–7460.
- [49] G. Cai, L. Xue, H. Zhang, J. Lin, A review on micromixers, *Micromachines* 8 (2017) 274.
- [50] S.T. Chang, E. Beaumont, D.N. Petsev, O.D. Velez, Remotely powered distributed microfluidic pumps and mixers based on miniature diodes, *Lab Chip* 8 (2008) 117–124.
- [51] K.S. Ryu, K. Shaikh, E. Goluch, Z. Fan, C. Liu, Micro magnetic stir-bar mixer integrated with parylene microfluidic channels, *Lab Chip* 4 (2004) 608–613.
- [52] C. Elbuken, T. Glawdel, D. Chan, C.L. Ren, Detection of microdroplet size and speed using capacitive sensors, *Sens. Actuators, A* 171 (2011) 55–62.
- [53] M. Marcali, C. Elbuken, Impedimetric detection and lumped element modelling of a hemagglutination assay in microdroplets, *Lab Chip* 16 (2016) 2494–2503.
- [54] B.J. Hindson, K.D. Ness, D.A. Masquelier, P. Belgrader, N.J. Heredia, A.J. Makarewicz, I.J. Bright, M.Y. Lucero, A.L. Hiddessen, T.C. Legler, High-throughput droplet digital PCR system for absolute quantitation of DNA copy number, *Anal. Chem.* 83 (2011) 8604–8610.
- [55] A. Kalantarifard, A. Saateh, C. Elbuken, Label-free sensing in microdroplet-based microfluidic systems, *Chemosensors* 6 (2018) 23.
- [56] T. Hong, A. Lu, W. Liu, C. Chen, Microdroplet synthesis of silver nanoparticles with controlled sizes, *Micromachines* 10 (2019) 274.